Parametric Mie resonances and directional amplification in time-modulated scatterers

V. Asadchy[1,2,†,*] A.G. Lamprianidis[3,*] G. Ptitcyn[2], M. Albooyeh[4], Rituraj[1,5], T. Karamanos[3], R. Alaee[3], S.A. Tretyakov[2], C. Rockstuhl[3,6], and S. Fan[1]

[1] *Ginzton Laboratory and Department of Electrical Engineering, Stanford University, Stanford, California 94305, USA*

[2] *Department of Electronics and Nanoengineering, Aalto University, P.O. Box 15500, FI-00076 Aalto, Finland*

[3] *Institute of Theoretical Solid State Physics, Karlsruhe Institute of Technology, 76131 Karlsruhe, Germany*

[4] *Mobix Labs Inc., 15420 Laguna Canyon, Irvine, California 92618, USA*

[5] *Department of Electrical Engineering, Indian Institute of Technology Kanpur, Kanpur-208016, UP, India*

[6] *Institute of Nanotechnology, Karlsruhe Institute of Technology, 76131 Karlsruhe, Germany*

[†] *email: viktar.asadchy@aalto.fi*

arXiv:2202.11138v2 [physics.optics] 22 Nov 2022

We provide a theoretical description of light scattering by a spherical particle whose permittivity is modulated in time at twice the frequency of the incident light. Such a particle acts as a finite-sized photonic time crystal and, despite its sub-wavelength spatial extent, can host optical parametric amplification. Conditions of parametric Mie resonances in the sphere are derived. We show that time-modulated materials provide a route to tailor directional light amplification, qualitatively different from that in scatterers made from a gain media. We design two characteristic time-modulated spheres that simultaneously exhibit light amplification and desired radiation patterns, including those with zero backward and/or vanishing forward scattering. The latter sphere provides an opportunity for creating shadow-free detectors of incident light.

I. INTRODUCTION

Sub-wavelength high-index dielectric resonators provide a versatile platform for light control at the nanoscale. These resonators can support strong light localization described by multipolar Mie-type resonances [1–6]. The resonant modes are generated by the volumetric distribution of displacement currents and can be of electric or magnetic kinds. A remarkable feature of Mie-type scattering lays in the possibility to spectrally overlap several multipolar modes for engineering complex scattering patterns. During the last few years, such multipolar mode engineering led to a number of applications in nanophotonics, including wavefront manipulations for metasurfaces [7], bound states in the continuum [8, 9], nonradiating anapole modes [10, 11], nanoparticle localization [12], and directional spontaneous parametric down-conversion [13, 14], among many others.

Most of the previous works on Mie-type scatterers concentrated on time-invariant particles whose permittivity *does not* change in time. The time variation of material properties unlocks an additional dimension of control in electromagnetic systems [15, 16]. Recently, a wide range of novel optical effects was suggested based on time-varying materials, such as photonic time crystals [17–22], temporal discontinuities [23–26], time-varying meta-atoms and antennas [27–31], effective magnetic field for photons [32], optically induced negative refraction [33], synthetic dimensions [34], etc. The temporal material modulation has the potential to dramatically extend both conceptual and applied aspects of Mie-type scattering [35, 36]. However, to date this area of research has remained essentially unexplored.

In this work, we analyse light scattering by a sphere whose permittivity is modulated at twice the frequency of the incident light, which corresponds to the case of parametric excitation. Based on Floquet-Mie theory and the temporal coupled mode theory, we demonstrate that such a sphere, despite its sub-wavelength spatial extend, hosts parametric Mie resonances. It is revealed that temporal modulations provide an additional design dimension, allowing directional light amplification by a scatterer. We highlight a qualitative difference of this mechanism from light amplification in scatterers with gain. We design two characteristic examples of parametric scatterers possessing finite light amplification with desired scattering patterns. A related effect of parametric amplification in spherical scatterers with the second-order nonlinearity was recently reported in Ref. [37], however, simultaneous far-field pattern engineering was not demonstrated.

II. BULK TIME-MODULATED MEDIUM

We consider a sphere located at the center of the coordinate system (see Fig. 1). The material of the sphere without modulations is described by a single-pole Lorentz-Drude dispersion model with the *stationary* relative permittivity function given by $\varepsilon_{\rm st}(\omega) = 1+\omega_{\rm p}^2/(\omega_{\rm r}^2 - \omega^2 - i\gamma\omega)$, where γ is the damping factor and $\omega_{\rm r}$ the resonance frequency. In what follows, we choose without loss of generality a plasma frequency of $\omega_{\rm p} = \sqrt{N_0 q_{\rm e}^2/m_{\rm e}\varepsilon_0} = 3.5\omega_{\rm r}$, where $q_{\rm e}$ and $m_{\rm e}$ are the electron charge and mass, respectively, and ε_0 is the vacuum permittivity. Parameter N_0 is the time-averaged bulk carrier density. The temporal variation of the sphere's permittivity ε is as-

[*] These authors contributed equally to this work

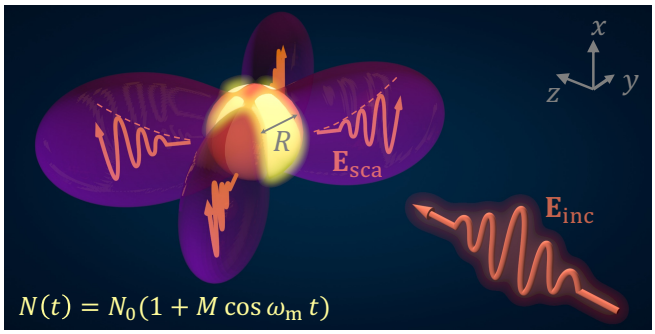


FIG. 1. Spherical particle with time-modulated bulk carrier density illuminated by incident light. Temporal modulation leads to parametric Mie resonances with simultaneous scattered-field amplification and possibility of far-field pattern manipulation.

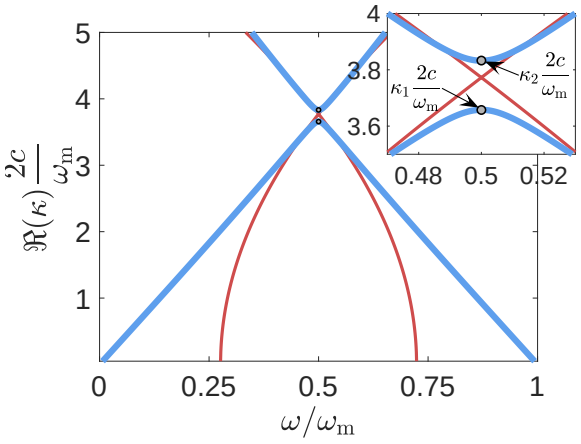


FIG. 2. Band structure diagram of a time-modulated material plotted for the case with modulation strength $M = 0.1$ and damping factor $\gamma = 0$ Hz. The thick blue and thin red lines correspond, respectively, to low- and high-frequency bulk plasmon-polariton bands in the Lorentzian dispersion.

sumed to be via the modulation of the charge carrier density of the form $N(t) = N_0(1 + M\cos\omega_{\rm m}t)$ (see Sec. 1 of the Supplemental Material [38]), where M is the modulation strength and $\omega_{\rm m}$ is the modulation frequency. In what follows, we choose a regime of relatively low dispersion, that is, $\omega_{\rm m} = 0.5\omega_{\rm r}$. Modulation of the carrier concentration with the strength of the order of unity and $\omega_{\rm m}$ at optical frequencies was experimentally demonstrated in several recent works [33, 39, 40].

We first find the eigenfrequencies and corresponding eigenmodes of an unbounded dispersive material with time-varying carrier concentration $N(t)$. The wave equation of such material written for the electric field $\mathbf{E}(\mathbf{r},\omega)$ reads [31, 36, 41]

$$\nabla\times\nabla\times\mathbf{E}(\mathbf{r},\omega) = k^2(\omega)\left[\mathbf{E}(\mathbf{r},\omega) + \int_{-\infty}^{+\infty}\chi(\omega-\omega',\omega')\mathbf{E}(\mathbf{r},\omega')\mathrm{d}\omega'\right]. \quad (1)$$

Here, $k(\omega) = \omega/c$ is the wavenumber of free space, c is the speed of light, $\mathbf{r}$ is the position vector, $\chi(\omega-\omega',\omega') = \varepsilon(\omega-\omega',\omega') - \delta(\omega-\omega')$ is the generalized susceptibility that describes the polarization density at frequency ω induced by an electric field harmonic at frequency ω', and $\delta(\omega-\omega')$ is the Dirac delta function. This susceptibility incorporates the information about the dynamics of the modulated medium and its dispersion properties [31, 42]. Solving the wave equation, we look for the electric field in the form $\mathbf{E}(\mathbf{r},\omega) = \int A(\kappa)S_\kappa(\omega)\mathbf{F}(\kappa\mathbf{r})\mathrm{d}\kappa$, where $A(\kappa)$ is the complex modal amplitude, and $S_\kappa(\omega)$ and $\mathbf{F}(\kappa\mathbf{r})$ are the spectral and spatial parts of the eigenmodes, respectively [36]. The latter is a solution of the Helmholtz wave equation with eigen-wavenumber κ.

By substituting the electric field ansatz into (1), we obtain the following eigenvalue equation in the matrix form (see Sec. 1 of the Supplemental Material [38]):

$$k_n^2(\varepsilon_{{\rm st},n}S_{\kappa,n} + \varepsilon_{{\rm dyn},n}S_{\kappa,n+1} + \varepsilon_{{\rm dyn},n}S_{\kappa,n-1}) = \kappa^2 S_{\kappa,n}, \quad (2)$$

where $\varepsilon_{\rm dyn}(\omega) = [\varepsilon_{\rm st}(\omega) - 1]M/2$ is the *dynamic* part of the relative permittivity. In (2), index n means that the corresponding function is taken at frequency $\omega_n = \omega + n\omega_{\rm m}$.

Equation (2) allows one to find a set of eigenwavenumbers κ_q (q is a positive integer) for a bulk temporally modulated material at a given Floquet frequency ω [18], as well as the matrix of weights S_{qn} of the modes with frequency ω_n and wavenumber κ_q. Eigenvalue equation (2) results in a band diagram with period $\omega_{\rm m}$ that corresponds to that of a photonic time crystal. Such a band diagram is dual (under replacement $\kappa \leftrightarrow \omega$) to that of conventional photonic crystals [43]. According to the duality with conventional photonic crystals, photonic time crystals can host momentum bandgaps. By solving eigenvalue equation (2) numerically, we are able to plot in Fig. 2 a band diagram of our photonic time crystal for the special case of the material with $M = 0.1$ and $\gamma = 0$ Hz (presence of a small nonzero γ leads to additional bands in the diagram but does not significantly modify the dispersion within the gap).

Since the considered material has a Lorentzian dispersion, there are two bulk plasmon-polariton bands where the real part of the permittivity is positive. These two bands are shown with blue and red lines in the figure. The first one (blue) is split by a momentum bandgap, inside which there are two modes which have purely imaginary eigenfrequencies (one attenuating and one amplifying) [20, 43, p. 53]. The amplifying mode is responsible for the parametric amplification effect in time-modulated materials and it is being excited even if the bandgap is closed by the red bands. The effect of the red bands in the scattering by the sphere can be neglected. Note that parametric amplification should be distinguished from optical gain that is modeled by a negative damping factor γ.

III. PARAMETRIC MIE RESONANCES IN TIME-MODULATED SPHERES

Next, we analyse wave phenomena in a finite-size sphere made from a time-modulated material. For clarity of the analysis, here we assume that temporal modulation inside the sphere are uniform. As we show in Sec. 3 of the Supplemental Material [38], possible spatial inhomogeneities of the sphere has only a minor quantitative impact on the results. First, we find the condition of optical parametric amplification. For its derivation, we will consider a separate eigenvalue problem for the electric field amplitudes across the sphere boundary with no incident field (parametric oscillations). To find the parametric oscillation condition analytically, we consider the Floquet frequency right at the center of the momentum bandgap, that is, $\omega = \omega_{\rm m}/2$, and exploit the weak-modulation approximation [44], which works perfectly in the regime of $M \ll 1$ and provides a very satisfactory estimation for $M < 0.2$ (see Fig. S2 in Sec. 5 of the Supplemental Material [38]). Here, we apply the approximation solely for the sake of making theoretical analysis more transparent for the reader and highlighting the qualitative picture of the considered phenomena. It is important to mention that one can also solve the eigenvalue equation (2) exactly, without resorting to any approximations, which will be done for the scatterer examples considered below. As we verified numerically, under this approximation, there are only two dominant harmonics $\omega_0 = \omega_{\rm m}/2$ and $\omega_{-1} = -\omega_{\rm m}/2$ and two dominant (lowest) momentum bands κ_1 and κ_2. In other words, the matrix of modal weights S_{qn} can be truncated to merely a 2×2 size with indices $q = \{1, 2\}$ and $n = \{0, -1\}$. The points with κ_1 and κ_2 are marked in the diagram of Fig. 2. Using the approximation, equation (2) can be solved analytically in a closed form (see Sec. 2 of the Supplemental Material [38]) yielding the following expressions for the momenta and modal weights for the parametric-oscillation regime:

$$\kappa_1 = \frac{\omega_{\rm m}}{2c}\sqrt{{\rm Re}\,\varepsilon_{{\rm st},0} - \tilde{\varepsilon}}, \quad \kappa_2 = \frac{\omega_{\rm m}}{2c}\sqrt{{\rm Re}\,\varepsilon_{{\rm st},0} + \tilde{\varepsilon}},$$
$$S_{qn} = \begin{pmatrix} \varepsilon^*_{{\rm dyn},0}/(i{\rm Im}\,\varepsilon_{{\rm st},0} - \tilde{\varepsilon}) & 1 \\ \varepsilon^*_{{\rm dyn},0}/(i{\rm Im}\,\varepsilon_{{\rm st},0} + \tilde{\varepsilon}) & 1 \end{pmatrix}, \tag{3}$$

where "$*$" denotes complex conjugation and $\tilde{\varepsilon} = \sqrt{|\varepsilon_{{\rm dyn},0}|^2 - ({\rm Im}\,\varepsilon_{{\rm st},0})^2}$. For the case when $\gamma = 0$ Hz, the matrix simplifies into $S_{qn} = [-1, 1; 1, 1]$ and the momentum bandgap width $\Delta\kappa = \kappa_2 - \kappa_1$ is linearly proportional to the modulation amplitude M:

$$\Delta\kappa = M\,\frac{\omega_{\rm m}}{4c}\,\frac{\omega_{\rm p}^2}{\sqrt{\omega_{\rm r}^2 - \omega_{\rm m}^2/4}\sqrt{\omega_{\rm r}^2 - \omega_{\rm m}^2/4 + \omega_{\rm p}^2}}. \tag{4}$$

Due to the spherical symmetry, the electric field inside the sphere can be expressed using a set of VSHs as $\mathbf{E}^{\rm in}(\mathbf{r}, \omega_n) = \sum_{\alpha,\mu,\nu,q} A^{\rm in}_{\alpha\mu\nu q}\,\mathbf{F}^{(1)}_{\alpha\mu\nu}(\kappa_q\mathbf{r})S_{qn}$, with $A^{\rm in}$ standing for amplitudes of corresponding VSHs with wavenumber κ_q. Here, indices μ and ν stand for the angular momentum along the z-axis and the multipolar order, respectively [36],[45, Sect. 13.3]. Subscript α stands for one of the two labels, α_M or α_N, and refers to magnetic or electric multipolar modes, respectively. Finally, superscript ι takes the values "1" or "3" to refer to regular or radiating VSHs, respectively. The electric field outside the sphere (in vacuum), represented by the scattered field only, is given by $\mathbf{E}^{\rm sca}(\mathbf{r}, \omega_n) = \sum_{\alpha,\mu,\nu} A^{\rm sca}_{\alpha\mu\nu}(\omega_n)\mathbf{F}^{(3)}_{\alpha\mu\nu}(k_n\mathbf{r})$. Importantly, here we are looking for the solution with no incident field present, which corresponds to the parametric oscillations regime. Next, we substitute these expressions into the boundary conditions at the surface of the sphere with radius R ($\mathbf{r} = R\,\hat{\mathbf{r}}$) [36]

$$\begin{aligned} \hat{\mathbf{r}} \times \left[\mathbf{E}^{\rm in}(\hat{\mathbf{r}}R, \omega_n) - \mathbf{E}^{\rm sca}(\hat{\mathbf{r}}R, \omega_n)\right] = 0, \\ \hat{\mathbf{r}} \times \left[\mathbf{H}^{\rm in}(\hat{\mathbf{r}}R, \omega_n) - \mathbf{H}^{\rm sca}(\hat{\mathbf{r}}R, \omega_n)\right] = 0, \end{aligned} \tag{5}$$

where $\hat{\mathbf{r}}$ is the radial unit vector and R is the radius of the sphere. Using the orthogonality relations for vector spherical harmonics [36], we obtain the following system of equations:

$$\begin{aligned} \sum_{q=1}^{2} A^{\rm in}_{\alpha\mu\nu q}\,S_{qn} z^{(1)}_{\alpha\nu}(\kappa_q R) = A^{\rm sca}_{\alpha\mu\nu}(\omega_n) z^{(3)}_{\alpha\nu}(k_n R), \\ \sum_{q=1}^{2} A^{\rm in}_{\alpha\mu\nu q}\,S_{qn}\kappa_q z^{(1)}_{\beta\nu}(\kappa_q R) = A^{\rm sca}_{\alpha\mu\nu}(\omega_n) k_n z^{(3)}_{\beta\nu}(k_n R). \end{aligned} \tag{6}$$

Here, index β is always different from α, that is, if $\alpha = \alpha_M$ then $\beta = \alpha_N$, and vice versa. Function $z^{(\iota)}_{\alpha_M\nu}$ denotes the spherical Bessel ($\iota = 1$) and Hankel ($\iota = 3$) functions of the first kind of order ν, while $z^{(\iota)}_{\alpha_N\nu}(x) = \frac{1}{x}\frac{\partial}{\partial x}[x z^{(\iota)}_{\alpha_M\nu}(x)]$. Equations (6) must hold for each set of parameters $\{\alpha, \mu, \nu, n\}$. Writing these two equations for the two frequency harmonics $n = 0$ and $n = -1$, we finally formulate the eigenvalue equation for the electric field amplitudes across the sphere boundary, i.e., with respect to field amplitudes $A^{\rm in}_{\alpha\mu\nu 1}$, $A^{\rm in}_{\alpha\mu\nu 2}$, $A^{\rm sca}_{\alpha\mu\nu}(\omega_{-1})$, and $A^{\rm sca}_{\alpha\mu\nu}(\omega_0)$. For the regime of parametric oscillations in the sphere (in the absence of incident waves), we are looking for the solutions with nonzero amplitudes $A^{\rm in}$ and $A^{\rm sca}$. Therefore, we equate the determinant of the 4×4 matrix in the eigenvalue problem to zero and solve the resulting equation with respect to the radius R and the modulation strength M of the sphere (see Sec. 2 of the Supplemental Material [38]).

Figure 3 depicts with colored lines the solutions of the zero matrix determinant for electric-type ($\alpha = \alpha_N$) and magnetic-type ($\alpha = \alpha_M$) modes in the sphere with multipolar orders from $\nu = 1$ to $\nu = 5$, indicating the threshold values of the modulation strength to provide parametric oscillations. The data are plotted for $\gamma = 0$ Hz. Nonzero dissipation would lead to merely a minor change in Fig. 3, shifting all the curves to the upper side. The

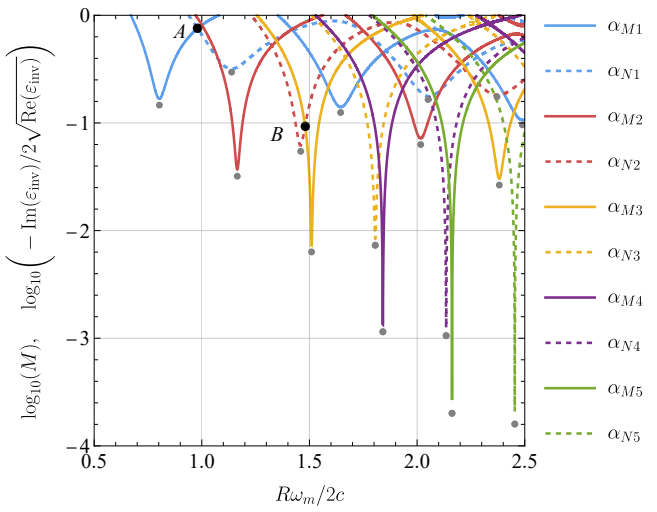


FIG. 3. The colored curves depict threshold values of the modulation strength M that provide parametric oscillations at fixed frequency $\omega_{\mathrm{m}}/2$ for different multipolar modes in a time-modulated sphere versus its normalized radius. The grey dots depict values of the normalized imaginary part of permittivity that support lasing at fixed frequency $\omega_{\mathrm{las}} = \omega_{\mathrm{m}}/2$ for different modes in a time-invariant sphere with optical gain. While horizontal coordinates of these points match to those of the minima of the colored curves for corresponding multipolar modes, their vertical coordinates do differ and the difference depends on the value of chosen stationary permittivity $\varepsilon_{\mathrm{st},0} = \mathrm{Re}(\varepsilon_{\mathrm{inv}})$ (see Sec. 4 of Supplemental Material [38]).

solutions are independent of parameter μ. The lines in the figure show all the sets of parameters (R and M) which yield parametric amplification of the corresponding multipolar mode in the time-modulated sphere. One can observe from the plot that higher-order multipolar modes (with larger values of $R\omega_{\mathrm{m}}/2c$ and higher quality factors) can host parametric oscillations at lower values of M. For example, the magnetic multipole of the order $\nu = 5$ ($\alpha = \alpha_{M5}$, green solid line) exhibits parametric oscillation at the value of M as low as 2.27×10^{-4}. The normalized radii $R\omega_{\mathrm{m}}/2c$ at the dips in Fig. 3 approximately coincide with those of conventional Mie resonances $R\omega_{\mathrm{Mie}}/c$ of the corresponding modes in a non-modulated sphere.

To analyse the physics of parametric Mie resonances, we employ a temporal coupled-mode theory [46–49]. Let us consider two coupled quasi-normal [50–52] modes inside the sphere at frequencies $\pm\omega_{\mathrm{m}}/2$ with the total electric field of the form $\mathbf{E}(\mathbf{r},t) = a_1(t)\,\mathrm{e}^{-i\omega_{\mathrm{m}}t/2}\,\mathbf{E}_{\mathrm{Mie}}(\mathbf{r}) + a_2(t)\,\mathrm{e}^{-i\omega_{\mathrm{m}}t/2}\,[\mathbf{E}_{\mathrm{Mie}}(\mathbf{r})]^* + \mathrm{c.c.}$ Here, $a_1(t)$ and $a_2(t)$ are the slowly varying temporal envelopes of the original and time-reversed modes and $\mathbf{E}_{\mathrm{Mie}}(\mathbf{r})$ is the spatial mode profile. We assume that $\omega_{\mathrm{m}}/2$ is close to the frequency ω_{Mie} that corresponds to one of the stationary Mie resonances, that is, $\omega_{\mathrm{Mie}} = \omega_{\mathrm{m}}/2 - \Delta\omega - i\gamma_{\mathrm{tot}}$ (where $|\Delta\omega + i\gamma_{\mathrm{tot}}| \ll \omega_{\mathrm{m}}/2$). Here, γ_{tot} is the total decay rate which includes radiation and possible dissipation losses (due to positive γ). Starting from the wave equation in the time-modulated material, one can arrive to the following system of coupled-mode equations describing evolution of mode envelopes $a_1(t)$ and $a_2^*(t)$ inside the sphere (see Sec. 3 of the Supplemental Material [38]):

$$\begin{aligned} \frac{\mathrm{d}}{\mathrm{d}t}a_1(t) &= [i\Delta\omega - \gamma_{\mathrm{tot}}]\,a_1(t) + i\eta a_2^*(t), \\ \frac{\mathrm{d}}{\mathrm{d}t}a_2^*(t) &= [-i\Delta\omega - \gamma_{\mathrm{tot}}]\,a_2^*(t) - i\eta^* a_1(t), \end{aligned} \tag{7}$$

where η is a coupling parameter linearly proportional to modulation strength M. Solving system (7), we obtain the threshold value of modulation strength $M_{\mathrm{thr}} \propto \gamma_{\mathrm{tot}} + \frac{1}{2\gamma_{\mathrm{tot}}}\Delta\omega^2$ for parametric amplification in the sphere. This value provides a qualitative description of the spectral lineshapes of the parametric Mie resonances (note that in Fig. 3 the logarithm of M is plotted). For modes with higher multipolar orders ν, the decay rate due to radiation loss γ_{tot} is smaller, which results in deeper dips.

As is seen from Fig. 3, the curves depicting the parametric oscillation condition at fixed frequency $\omega_{\mathrm{m}}/2$ are continuous. This feature allows us to select the sphere configuration with M and R at the points where the curves intersect such that simultaneous parametric amplification of two desired multipolar modes occurs at the same frequency (ensuring coherence). The orientation of these modes is locked when the sphere is illuminated by incident light. By choosing the pair of modes, one can control the radiation pattern of the amplified scattered light. Importantly, such a multi-mode coherent amplification regime is not accessible in time-invariant spheres made from a medium with gain [53]. In order to demonstrate this, we additionally mark with grey dots in Fig. 3 those configurations of such an active sphere (with radius R and complex time-invariant permittivity $\varepsilon_{\mathrm{inv}}$) that support lasing (divergent scattering cross section) for different modes at the fixed frequency $\omega_{\mathrm{las}} = \omega_{\mathrm{m}}/2$. For fair comparison, we choose $\mathrm{Re}(\varepsilon_{\mathrm{inv}}) = \varepsilon_{\mathrm{st},0}$. The details of the calculations as well as comparison for other values of $\mathrm{Re}(\varepsilon_{\mathrm{inv}})$ can be found in Sec. 4 of Supplemental Material [38]. As is seen, lasing in time-invariant spheres occurs only at discrete points in the configuration space, and simultaneous satisfaction of the lasing condition for several modes at the same frequency is generally impossible. Such qualitatively different behaviour suggests that temporal modulations provide a pathway for achieving coherent amplification by the sphere with desired radiation pattern. Moreover, due to a finite width of each dip in Fig. 3, it is possible to excite higher-order multipolar modes in a sphere of smaller size compared to that in the absence of temporal modulations [27].

IV. SCATTERING FROM TIME-MODULATED SPHERES

In order to demonstrate the potential of directional amplification, next we consider two representative ex-

amples of parametric spheres. In both examples the sphere is illuminated by monochromatic plane waves at a frequency $\omega_{\rm inc}$ (see Fig. 1). The incident frequency is slightly shifted away from $\omega_{\rm m}/2$ so that we can achieve finite and controllable amplification and use the harmonic-field analysis. From a practical point of view, the amplification can be locked-in to frequency $\omega_{\rm inc}$ instead of $\omega_{\rm m}/2$ if temporal modulations occur while the sphere is illuminated by the incident light [54].

Designing the radiation pattern of a particle near the lasing condition (near parametric oscillation) is challenging. Whereas the lasing occurs for each multipole independently, we need to obtain the superposition of multipoles of comparable strength and with appropriate phases to achieve a desired radiation pattern. However, the lasing multipoles have diverging amplitudes and therefore dominate the radiation pattern, rendering the contributions of the rest of the radiating multipoles insignificant upon a superposition. Therefore, the simultaneous satisfaction of the lasing condition for several multipoles is needed to shape the radiation pattern of a lasing particle. Fine tuning the system at the vicinity of the parameter space, where such an overlap of parametric Mie resonances happens, allows for the engineering of the relative amplitudes and phases of each lasing multipole, finally leading to the engineering of a lasing particle with a desired radiation pattern.

For the first example, we consider a sphere configuration with $M = 0.68$ and $R = 1.048\frac{2c}{\omega_{\rm m}}$, marked by point A in Fig. 3. The configuration corresponds to the first parametric resonance crossing of the electric and magnetic dipole modes. Since contours in Fig. 3 were plotted under the approximation of $M \ll 1$, for finding the exact coordinates of point A, we calculated the contours considering a large number of frequency harmonics (see Sec. 5 in Supplemental Material [38]). In the present and the following examples, we chose $\gamma = 0$ Hz. We excite the sphere by incident light at $\omega_{\rm inc} = 0.498\omega_{\rm m}$. To find the scattered fields, we use the eigenvalue equation (2), the boundary conditions which include the incident fields, and the expansion of the fields in series of radiating VSHs (see Sec. 6 in Supplemental Material [38]). Figure 4(a) depicts the scattered far-field pattern at frequency $\omega_{\rm inc}$. The pattern is unidirectional, revealing zero backward scattering due to close fulfillment of the first Kerker condition [55]. The condition implies that the electric and magnetic modes in the sphere have approximately same amplitudes and phases. We were able to reach such a balance by fine adjustments of parameters M, R, and $\omega_{\rm inc}$. Interestingly, we observed that having a non-zero damping factor γ in the material of the sphere precludes achieving exact zero backward scattering, which is in agreement with recent similar findings for time-invariant lossy uniform spheres [53, 56]. While in [53] it was proved that ideal zero backward scattering cannot occur in spheres with *optical gain*, this statement does not apply to the time-modulated spheres with *parametric gain* considered in this work. The scattering and absorption cross sections in this example are $C_{\rm sca}/C_{\rm geom} = 2629.2$ and $C_{\rm abs}/C_{\rm geom} = -2627.5$, where $C_{\rm geom} = \pi R^2$ and negative sign of $C_{\rm abs}$ implies the activity of the modulated sphere. Clearly, the scattering cross section largely exceeds that of the same sphere without temporal modulations (for which case $C^{\rm st}_{\rm sca}/C_{\rm geom} = 5.5$ and $C^{\rm st}_{\rm abs} = 0$) due to the presence of modulation.

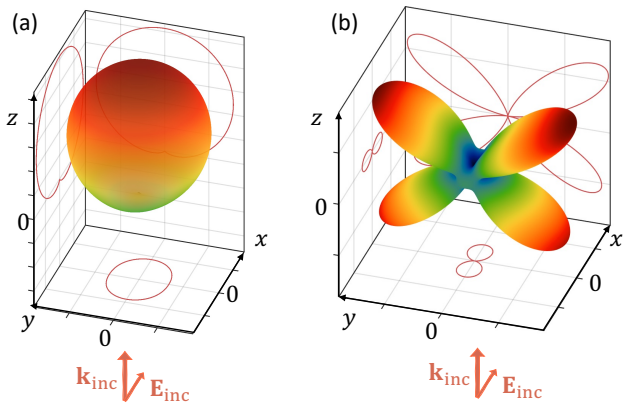


FIG. 4. Scattered far-field patterns of time-modulated spheres with parameters (a) $M = 0.68$ and $R = 1.048\frac{2c}{\omega_{\rm m}}$ and (b) $M = 0.093$ and $R = 1.481\frac{2c}{\omega_{\rm m}}$. The patterns are calculated at the frequency of incident wave $\omega_{\rm inc}$. The red contours depict cross sections of the patterns parallel to the xy, yz, and xz planes, calculated at the center of the coordinate system. The colors of the patterns denote the scattering amplitude (dark red and dark blue colors stand for the maximum and minimum values, respectively).

The second example is a sphere with a configuration of $M = 0.093$ and $R = 1.481\frac{2c}{\omega_{\rm m}}$ (see point B in Fig. 3) which coincides with the parametric resonance crossing of the electric quadrupole and magnetic octupole modes. Incident light at $\omega_{\rm inc} = 0.4995\omega_{\rm m}$ is scattered by the sphere with the pattern shown in Fig. 4(b). The pattern has sharp dips in both the backward and forward directions. Note that, whereas the electric and magnetic dipoles have opposite parity symmetry, ensuring the first Kerker condition, the electric quadrupole and magnetic octupole have the same parity symmetry, allowing for the engineering of both the first and second Kerker conditions simultaneously [55]. The scattering and absorption cross sections are $C_{\rm sca}/C_{\rm geom} = 858.3$ and $C_{\rm abs}/C_{\rm geom} = -857.5$ (in comparison, $C^{\rm st}_{\rm sca}/C_{\rm geom} = 2.53$ and $C^{\rm st}_{\rm abs} = 0$ for the stationary sphere). For both considered time-modulated spheres, the optical theorem [57], written for the forward scattering and extinction cross section at the fundamental frequency $\omega_{\rm inc}$, is satisfied. The peculiar pattern in Fig. 4(b) with scattering dips in both forward and backward directions stems from the precise engineering of amplitude and phases of the two multipolar modes (see Sec. 6 of the Supplemental Material [38] and [58]).

V. DISCUSSION

We have explored optical parametric amplification by spherical scatterers with time-modulated permittivity. The presented two example geometries highlight the fascinating opportunities of simultaneous light amplification and scattering pattern control provided by the additional temporal dimension. Indeed, the second sphere example provides an interesting functionality: shadow-free detection of incident light due to vanishing forward scattering (related concept using active and parity-time-symmetric dimers was suggested in [59, 60]). The sphere scatters light sideways where it can be detected by sensors. Parametric amplification enables detection of extremely weak signals. Due to the symmetry of the sphere, it is possible to determine also the propagation direction of the light under detection by looking at the scattering pattern. Furthermore, time-modulated particles can find applications for designing nanoscale amplifiers. Due to the directional nature of their scattering and possibility of finite amplification, one can create exotic non-attenuating waveguide modes and topological edge modes in a non-uniform lattice of such spheres. Our results can be extended to other domains (acoustics, water waves, etc.), to particles with other geometries, and represent the first step towards parametric metasurfaces based on time-modulated scatterers.

ACKNOWLEDGMENT

This work was supported by the MURI project from the U.S. Air Force of Office of Scientific Research (Grant No FA9550-21-1-0244), German Research Foundation through Germany's Excellence Strategy via the Excellence Cluster 3D Matter Made to Order (EXC- 2082/1 - 390761711), Alexander von Humboldt Foundation, and the Academy of Finland (project 330260). A. G. L. acknowledges support from the Max Planck School of Photonics, which is supported by BMBF, Max Planck Society, and Fraunhofer Society and from the Karlsruhe School of Optics and Photonics (KSOP).

[1] M. I. Mishchenko, L. D. Travis, and A. A. Lacis, *Scattering, Absorption, and Emission of Light by Small Particles* (Cambridge University Press, 2002).
[2] C. F. Bohren and D. R. Huffman, *Absorption and Scattering of Light by Small Particles* (John Wiley & Sons, 2008).
[3] S. Kruk and Y. Kivshar, Functional meta-optics and nanophotonics governed by Mie resonances, ACS Photonics **4**, 2638 (2017).
[4] W. Liu and Y. S. Kivshar, Generalized Kerker effects in nanophotonics and meta-optics, Optics Express **26**, 13085 (2018).
[5] D. Tzarouchis and A. Sihvola, Light scattering by a dielectric sphere: Perspectives on the Mie resonances, Applied Sciences **8**, 184 (2018).
[6] K. Koshelev and Y. Kivshar, Dielectric resonant metaphotonics, ACS Photonics **8**, 102 (2021).
[7] M. Decker, I. Staude, M. Falkner, J. Dominguez, D. N. Neshev, I. Brener, T. Pertsch, and Y. S. Kivshar, High-efficiency dielectric Huygens' surfaces, Advanced Optical Materials **3**, 813 (2015).
[8] C. W. Hsu, B. Zhen, A. D. Stone, J. D. Joannopoulos, and M. Soljačić, Bound states in the continuum, Nature Reviews Materials **1**, 1 (2016).
[9] K. Koshelev, S. Lepeshov, M. Liu, A. Bogdanov, and Y. Kivshar, Asymmetric metasurfaces with high-Q resonances governed by bound states in the continuum, Physical Review Letters **121**, 193903 (2018).
[10] A. J. Devaney and E. Wolf, Radiating and nonradiating classical current distributions and the fields they generate, Physical Review D **8**, 1044 (1973).
[11] A. E. Miroshnichenko, A. B. Evlyukhin, Y. F. Yu, R. M. Bakker, A. Chipouline, A. I. Kuznetsov, B. Luk'yanchuk, B. N. Chichkov, and Y. S. Kivshar, Nonradiating anapole modes in dielectric nanoparticles, Nature Communications **6**, 8069 (2015).
[12] A. Bag, M. Neugebauer, P. Woźniak, G. Leuchs, and P. Banzer, Transverse Kerker scattering for angstrom localization of nanoparticles, Physical Review Letters **121**, 193902 (2018).
[13] G. Marino, A. S. Solntsev, L. Xu, V. F. Gili, L. Carletti, A. N. Poddubny, M. Rahmani, D. A. Smirnova, H. Chen, A. Lemaître, G. Zhang, A. V. Zayats, C. D. Angelis, G. Leo, A. A. Sukhorukov, and D. N. Neshev, Spontaneous photon-pair generation from a dielectric nanoantenna, Optica **6**, 1416 (2019).
[14] A. Nikolaeva, K. Frizyuk, N. Olekhno, A. Solntsev, and M. Petrov, Directional emission of down-converted photons from a dielectric nanoresonator, Physical Review A **103**, 043703 (2021).
[15] N. Engheta, Metamaterials with high degrees of freedom: Space, time, and more, Nanophotonics **10**, 639 (2021).
[16] E. Galiffi, R. Tirole, S. Yin, H. Li, S. Vezzoli, P. A. Huidobro, M. G. Silveirinha, R. Sapienza, A. Alù, and J. B. Pendry, Photonics of time-varying media, Advanced Photonics **4**, 014002 (2022).
[17] F. Biancalana, A. Amann, A. V. Uskov, and E. P. O'Reilly, Dynamics of light propagation in spatiotemporal dielectric structures, Physical Review E **75**, 046607 (2007).
[18] J. R. Zurita-Sánchez, P. Halevi, and J. C. Cervantes-Gonzalez, Reflection and transmission of a wave incident on a slab with a time-periodic dielectric function $\varepsilon(t)$, Physical Review A **79**, 053821 (2009).
[19] J. R. Reyes-Ayona and P. Halevi, Observation of genuine wave vector (k or β) gap in a dynamic transmission line and temporal photonic crystals, Applied Physics Letters **107**, 074101 (2015).
[20] E. Lustig, Y. Sharabi, and M. Segev, Topological aspects of photonic time crystals, Optica **5**, 1390 (2018).

[21] J. Park and B. Min, Spatiotemporal plane wave expansion method for arbitrary space–time periodic photonic media, Optics Letters **46**, 484 (2021).

[22] Y. Sharabi, E. Lustig, and M. Segev, Disordered photonic time crystals, Physical Review Letters **126**, 163902 (2021).

[23] Y. Zhou, M. Z. Alam, M. Karimi, J. Upham, O. Reshef, C. Liu, A. E. Willner, and R. W. Boyd, Broadband frequency translation through time refraction in an epsilon-near-zero material, Nature Communications **11**, 2180 (2020).

[24] V. Pacheco-Peña and N. Engheta, Antireflection temporal coatings, Optica **7**, 323 (2020).

[25] R. A. C. Quiñones, T. C. Underwood, and M. A. Cappelli, Tunable surface plasmon resonance in laser-induced plasma spheroids, Plasma Sources Science and Technology **30**, 045010 (2021).

[26] S. Yin and A. Alù, Efficient phase conjugation in a space-time leaky waveguide, ACS Photonics **9**, 979 (2022).

[27] A. Salandrino, Plasmonic parametric resonance, Physical Review B **97**, 081401 (2018).

[28] M. S. Mirmoosa, M. S. M. Mollaei, G. A. Ptitcyn, C. R. Simovski, and S. A. Tretyakov, Time-varying plasmonic particles, in *2021 Fifteenth International Congress on Artificial Materials for Novel Wave Phenomena (Metamaterials)* (2021) pp. 272–274.

[29] D. M. Solís and N. Engheta, Functional analysis of the polarization response in linear time-varying media: A generalization of the Kramers-Kronig relations, Physical Review B **103**, 144303 (2021).

[30] A. Mekawy, H. Li, Y. Radi, and A. Alù, Parametric enhancement of radiation from electrically small antennas, Physical Review Applied **15**, 054063 (2021).

[31] M. S. Mirmoosa, T. T. Koutserimpas, G. A. Ptitcyn, S. A. Tretyakov, and R. Fleury, Dipole polarizability of time-varying particles, New Journal of Physics **24**, 063004 (2022).

[32] K. Fang, Z. Yu, and S. Fan, Realizing effective magnetic field for photons by controlling the phase of dynamic modulation, Nature Photonics **6**, 782 (2012).

[33] S. Vezzoli, V. Bruno, C. DeVault, T. Roger, V. M. Shalaev, A. Boltasseva, M. Ferrera, M. Clerici, A. Dubietis, and D. Faccio, Optical time reversal from time-dependent epsilon-near-zero media, Physical Review Letters **120**, 043902 (2018).

[34] L. Yuan, A. Dutt, and S. Fan, Synthetic frequency dimensions in dynamically modulated ring resonators, APL Photonics **6**, 071102 (2021).

[35] I. Stefanou, P. A. Pantazopoulos, and N. Stefanou, Light scattering by a spherical particle with a time-periodic refractive index, JOSA B **38**, 407 (2021).

[36] G. Ptitcyn, A. G. Lamprianidis, T. Karamanos, V. S. Asadchy, R. Alaee, M. Müller, M. Albooyeh, M. S. Mirmoosa, S. Fan, S. A. Tretyakov, and C. Rockstuhl, Scattering from spheres made of time-varying and dispersive materials, arXiv:2110.07195 [physics] (2021).

[37] S. Jahani, A. Roy, and A. Marandi, Wavelength-scale optical parametric oscillators, Optica **8**, 262 (2021).

[38] See Supplemental Material for additional information.

[39] M. Z. Alam, I. De Leon, and R. W. Boyd, Large optical nonlinearity of indium tin oxide in its epsilon-near-zero region, Science **352**, 795 (2016).

[40] L. Caspani, R. Kaipurath, M. Clerici, M. Ferrera, T. Roger, J. Kim, N. Kinsey, M. Pietrzyk, A. Di Falco, V. Shalaev, A. Boltasseva, and D. Faccio, Enhanced nonlinear refractive index in ε-near-zero materials, Physical Review Letters **116**, 233901 (2016).

[41] Y. Shi, W. Shin, and S. Fan, Multi-frequency finite-difference frequency-domain algorithm for active nanophotonic device simulations, Optica **3**, 1256 (2016).

[42] D. M. Solís, R. Kastner, R. Kastner, and N. Engheta, Time-varying materials in the presence of dispersion: Plane-wave propagation in a Lorentzian medium with temporal discontinuity, Photonics Research **9**, 1842 (2021).

[43] J. D. Joannopoulos, S. G. Johnson, J. N. Winn, and R. D. Meade, *Photonic Crystals: Molding the Flow of Light* (Princeton University Press, 2011).

[44] J. S. Martínez-Romero and P. Halevi, Parametric resonances in a temporal photonic crystal slab, Physical Review A **98**, 053852 (2018).

[45] P. Morse and H. Feshbach, *Methods of Theoretical Physics*, International series in pure and applied physics (McGraw-Hill, 1953).

[46] H. A. Haus, *Waves and Fields in Optoelectronics* (Prentice-Hall, 1984).

[47] H. A. Haus, *Electromagnetic Noise and Quantum Optical Measurements* (Springer Science & Business Media, 2012).

[48] A. Rodriguez, M. Soljačić, J. D. Joannopoulos, and S. G. Johnson, $\chi^{(2)}$ and $\chi^{(3)}$ harmonic generation at a critical power in inhomogeneous doubly resonant cavities, Optics Express **15**, 7303 (2007).

[49] S. Fan, 12 - Photonic crystal theory: Temporal coupled-mode formalism, in *Optical Fiber Telecommunications V A*, Optics and Photonics, edited by I. P. Kaminow, T. Li, and A. E. Willner (Academic Press, Burlington, 2008) 5th ed., pp. 431–454.

[50] M. B. Doost, W. Langbein, and E. A. Muljarov, Resonant-state expansion applied to three-dimensional open optical systems, Physical Review A **90**, 013834 (2014).

[51] T. Wu, A. Baron, P. Lalanne, and K. Vynck, Intrinsic multipolar contents of nanoresonators for tailored scattering, Phys. Rev. A **101**, 011803 (2020).

[52] S. Gladyshev, K. Frizyuk, and A. Bogdanov, Symmetry analysis and multipole classification of eigenmodes in electromagnetic resonators for engineering their optical properties, Phys. Rev. B **102**, 075103 (2020).

[53] J. Olmos-Trigo, C. Sanz-Fernández, D. R. Abujetas, J. Lasa-Alonso, N. de Sousa, A. García-Etxarri, J. A. Sánchez-Gil, G. Molina-Terriza, and J. J. Sáenz, Kerker conditions upon lossless, absorption, and optical gain regimes, Physical Review Letters **125**, 073205 (2020).

[54] R. W. Boyd, *Nonlinear Optics* (Academic Press, 2020).

[55] M. Kerker, D.-S. Wang, and C. L. Giles, Electromagnetic scattering by magnetic spheres, Journal of the Optical Society of America **73**, 765 (1983).

[56] J. Olmos-Trigo, D. R. Abujetas, C. Sanz-Fernández, J. A. Sánchez-Gil, and J. J. Sáenz, Optimal backward light scattering by dipolar particles, Physical Review Research **2**, 013225 (2020).

[57] R. G. Newton, Optical theorem and beyond, American Journal of Physics **44**, 639 (1976).

[58] J. Y. Lee, A. E. Miroshnichenko, and R.-K. Lee, Simultaneously nearly zero forward and nearly zero backward scattering objects, Optics Express **26**, 30393 (2018).

[59] R. Fleury, D. Sounas, and A. Alù, An invisible acoustic sensor based on parity-time symmetry, Nature Communications **6**, 5905 (2015).

[60] M. Safari, M. Albooyeh, C. R. Simovski, and S. A. Tretyakov, Shadow-free multimers as extreme-performance meta-atoms, Physical Review B **97**, 085412 (2018).